A Fault-Location Method for Application With Current Differential Relays of Three-Terminal Lines

Jan Izykowski, *Senior Member, IEEE*, Eugeniusz Rosolowski, *Senior Member, IEEE*, Murari Mohan Saha, *Senior Member, IEEE*, Marek Fulczyk, *Member, IEEE*, and Przemyslaw Balcerek

***Abstract*—This paper presents a new method for locating faults on three-terminal power lines. Estimation of a distance to fault and indication of a faulted section is performed using three-phase current from all three terminals and additionally three-phase voltage from the terminal at which a fault locator is installed. Such a set of synchronized measurements has been taken into consideration with the aim of developing a fault-location algorithm for applications with current differential relays of three-terminal lines. The delivered fault-location algorithm consists of three subroutines designated for locating faults within particular line sections and a procedure for indicating the faulted line section. Testing and evaluation of the algorithm has been performed with fault data obtained from versatile Alternate Transients Program–Electromagnetic Transients Program simulations. The sample results of the evaluation are reported and discussed.**

***Index Terms*—Alternate Transients Program (ATP)–Electromagnetic Transients Program (EMTP), current differential relay, fault location, simulation, synchronized phasor measurement, three-terminal line.**

I. Introduction

ACCURATE location of faults on overhead power lines for inspection-repair purposes [1]–[12] is of vital importance for operators and the utility staff for expediting service restoration and, thus, to reduce outage time, operating costs, and customer complains.

An impedance principle, making use of the fundamental frequency voltages and currents [3]–[9], and traveling-wave approach [10] have been developed so far for applications to three-terminal lines.

In [3], the use of synchronized measurements of currents and voltages from all three terminals has been considered. Distributed parameter models of the line sections have been utilized there. This ensures high accuracy of fault location and the faulted line section is also reliably indicated [3].

Use of three-end unsynchronized measurements of current and voltage has been considered in [4]. The lumped models of the line sections were applied there and it was also implied that the error resulting from such simplification is minimized due to the redundancy of the fault-location equations. Yet another utilization of three-end unsynchronized measurements has been proposed in [5], where exchanging the minimal amount of information between the line terminals over a protection channel was considered.

In turn, the demand and importance of developing fault-location algorithms for three-terminal lines utilizing only two-end synchronized measurements of voltages and currents has been stated in [6]. This is required since the measurement infrastructure of the tapping line could be poor or there is no available communication channel for sending measurements from the far end of the tapping line.

Limited availability of measurements for fault location on three-terminal lines was considered in [7]–[9]. In particular, the approaches introduced in [7] and [8] ensure complete immunity to saturation of current transformers (CTs), since only voltage signals are utilized for fault location. The other method, delivered in [9], is based on using minimal measurements (i.e., the one-end measurement of three-phase voltage and current), supplemented with additional information on amplitudes of prefault currents in a three-terminal line.

Use of yet another set of the fault-locator input signals, which differs from those applied in the cited approaches [3]–[9] is proposed in this paper. Three-phase current from all three line terminals and additionally three-phase voltage, acquired at the terminal at which the fault locator is installed, are taken into consideration. Such specific availability of measurements for locating faults has been assumed with the aim of simply adding the fault-location function to current differential relays protecting three-terminal lines [13].

After derivation of the complete fault-location algorithm, the results of its evaluation with the use of the ATP–EMTP [14] simulation data are delivered and discussed.

II. Fault-Location Technique

Modern microprocessor-based current differential relays exchange the digital forms of the locally measured current phasors even over long distances. For this purpose, different forms of communication means are utilized. The current differential protection principle requires synchronization of digital measurements performed at different line terminals. This is accomplished using the well-known global positioning system (GPS) or the other techniques [13].

It is considered further that the fault-location (FL) function is supplemented to the current differential relay from substation A

Manuscript received July 20, 2006; revised January 10, 2007. This work was supported in part by ABB Corporate Research Center in Krakow, Poland, and in part by the Ministry of Science and Higher Education of Poland under Grant 3 T10B 070 30. Paper no. TPWRD-00402-2006.

J. Izykowski and E. Rosolowski are with the Wroclaw University of Technology, Wroclaw 50-370, Poland (e-mail: jan.izykowski@pwr.wroc.pl; eugeniusz.rosolowski@pwr.wroc.pl).

M. M. Saha is with ABB, Västeras SE-721 59, Sweden (e-mail: murari.saha@se.abb.com).

M. Fulczyk and P. Balcerek are with ABB Corporate Research Center, Krakow 31-038, Poland (e-mail: marek.fulczyk@pl.abb.com; przemyslaw.balcerek@pl.abb.com).

Digital Object Identifier 10.1109/TPWRD.2007.905544

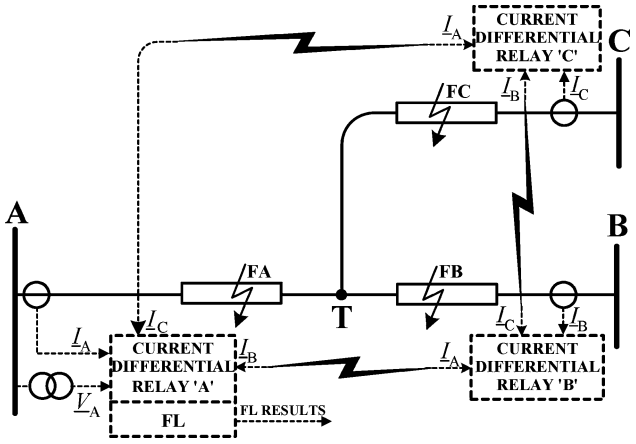

Fig. 1. Fault location on a three-terminal line associated with current differential relays.

(Fig. 1). For this purpose, phasors of three-phase current from all line terminals $\underline{I}_{\mathrm{A}}, \underline{I}_{\mathrm{B}}, \underline{I}_{\mathrm{C}}$—exchanged by the current differential relays A, B, and C, together with the locally measured three-phase voltage phasor $(\underline{V}_{\mathrm{A}})$, are taken as the fault-locator input signals. In a natural way, these measurements are further considered as being synchronized.

The proposed fault-location technique is based on using three subroutines, denoted further as SUB_A, SUB_B, and SUB_C. They are designated for locating faults FA, FB, and FC at hypothetical fault spots within particular line sections: AT, TB, TC, respectively. It is worth realizing that the position of a fault is a random factor and, thus, the faulted line section is not known in advance. Therefore, the valid subroutine will be chosen by using a special selection procedure.

A. *Fault-Location Algorithm—Subroutine SUB_A*

The subroutine SUB_A, designed for locating faults (FA) within the line section AT (Fig. 2), is based on the following generalized fault-loop model [12]:

$$\underline{V}_{\mathrm{Ap}} - d_{\mathrm{A}}\underline{Z}_{1\mathrm{LA}}\underline{I}_{\mathrm{Ap}} - R_{\mathrm{FA}}\underline{I}_{\mathrm{F}} = 0 \tag{1}$$

where

d_{A}	unknown distance to fault on section AT (p.u.);
R_{FA}	unknown fault resistance;
$\underline{V}_{\mathrm{Ap}}, \underline{I}_{\mathrm{Ap}}$	fault-loop voltage and current;
$\underline{Z}_{1\mathrm{LA}}$	positive-sequence impedance of the section AT;
$\underline{I}_{\mathrm{F}}$	total fault current (fault path current).

Fault-loop voltage and current are composed accordingly to the fault type, as the following weighted sums of the respective symmetrical components of the measured signals:

$$\underline{V}_{\mathrm{Ap}} = \underline{a}_1\underline{V}_{\mathrm{A1}} + \underline{a}_2\underline{V}_{\mathrm{A2}} + \underline{a}_0\underline{V}_{\mathrm{A0}} \tag{2}$$

$$\underline{I}_{\mathrm{Ap}} = \underline{a}_1\underline{I}_{\mathrm{A1}} + \underline{a}_2\underline{I}_{\mathrm{A2}} + \underline{a}_0\frac{\underline{Z}_{0\mathrm{LA}}}{\underline{Z}_{1\mathrm{LA}}}\underline{I}_{\mathrm{A0}} \tag{3}$$

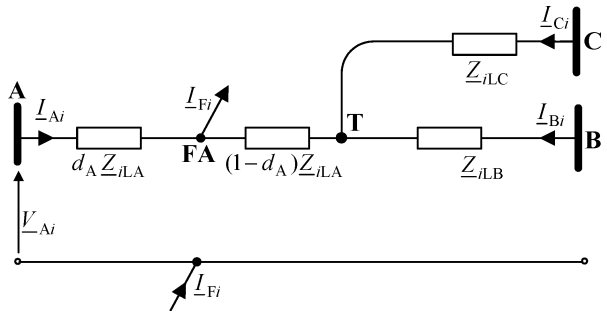

Fig. 2. Circuit diagram of the three-terminal line under fault at section AT, for the ith symmetrical component.

TABLE I
WEIGHTING COEFFICIENTS FOR COMPOSING FAULT-LOOP SIGNALS (2), (3)

FAULT	$\underline{a}_1$	$\underline{a}_2$	$\underline{a}_0$
a-g	1	1	1
b-g	$-0.5 - \mathrm{j}0.5\sqrt{3}$	$0.5 + \mathrm{j}0.5\sqrt{3}$	1
c-g	$0.5 + \mathrm{j}0.5\sqrt{3}$	$-0.5 - \mathrm{j}0.5\sqrt{3}$	1
a-b, a-b-g a-b-c, a-b-c-g	$1.5 + \mathrm{j}0.5\sqrt{3}$	$1.5 - \mathrm{j}0.5\sqrt{3}$	0
b-c, b-c-g	$-\mathrm{j}\sqrt{3}$	$\mathrm{j}\sqrt{3}$	0
c-a, c-a-g	$-1.5 + \mathrm{j}0.5\sqrt{3}$	$-1.5 - \mathrm{j}0.5\sqrt{3}$	0

where

$\underline{a}_1, \underline{a}_2, \underline{a}_0$	weighting coefficients;
$\underline{V}_{\mathrm{A1}}, \underline{V}_{\mathrm{A2}}, \underline{V}_{\mathrm{A0}}$	symmetrical components of side A voltages;
$\underline{I}_{\mathrm{A1}}, \underline{I}_{\mathrm{A2}}, \underline{I}_{\mathrm{A0}}$	symmetrical components of side A currents;
$\underline{Z}_{0\mathrm{LA}}$	zero-sequence impedance of the line section AT.

Fault-loop signals (2) and (3), and also those used in the remaining subroutines, are expressed in terms of the respective symmetrical components. Use of such notation is convenient for introducing the compensation for line shunt capacitances; however, it is fully equivalent to the description traditionally used for distance protection [12]. The natural sequence of phases: a, b, and c was assumed for determining the weighting coefficients (Table I) as well as in all further symmetrical components calculations.

It is proposed to calculate the total fault current from (1) using the following generalized fault model:

$$\underline{I}_{\mathrm{F}} = \underline{a}_{\mathrm{F1}}\underline{I}_{\mathrm{F1}} + \underline{a}_{\mathrm{F2}}\underline{I}_{\mathrm{F2}} + \underline{a}_{\mathrm{F0}}\underline{I}_{\mathrm{F0}} \tag{4}$$

where

$\underline{a}_{\mathrm{F1}}, \underline{a}_{\mathrm{F2}}, \underline{a}_{\mathrm{F0}}$	share coefficients (Table II).

The ith sequence component of the total fault current is determined as a sum of the ith sequence components of currents from all line terminals (A, B, C)

$$\underline{I}_{\mathrm{F}i} = \underline{I}_{\mathrm{A}i} + \underline{I}_{\mathrm{B}i} + \underline{I}_{\mathrm{C}i} \tag{5}$$

TABLE II
SHARE COEFFICIENTS USED IN FAULT MODEL (4)

FAULT	$\underline{a}_{F1}$	$\underline{a}_{F2}$	$\underline{a}_{F0}$
a-g	0	3	0
b-g	0	$1.5+j1.5\sqrt{3}$	0
c-g	0	$-1.5-j1.5\sqrt{3}$	0
a-b	0	$1.5-j0.5\sqrt{3}$	0
b-c	0	$j\sqrt{3}$	0
c-a	0	$-1.5-j0.5\sqrt{3}$	0
a-b-g	0	$3-j\sqrt{3}$	$j\sqrt{3}$
b-c-g	0	$j2\sqrt{3}$	$j\sqrt{3}$
c-a-g	0	$-3-j\sqrt{3}$	$j\sqrt{3}$
a-b-c a-b-c-g	$1.5+j0.5\sqrt{3}$	$1.5-j0.5\sqrt{3}$ *)	0
*) $\underline{a}_{F2} \neq 0$, however, negative sequence component is not present under three-phase balanced faults.			

where

subscript "i" denotes the component type: $i = 1$—positive, $i = 2$—negative, and $i = 0$—zero sequence.

The share coefficients from (4) can be determined by performing an analysis of the boundary conditions for particular fault types [12]. Different sets of those coefficients are obtained. They can be used alternatively, however, in order to ensure high accuracy of fault location and the following priority for the use of particular sequence components of measured currents is proposed (Table II):

- for phase-to-ground and phase-to-phase faults: use of negative-sequence components;
- for phase-to-phase-to-ground faults: use of negative- and zero-sequence components;
- for three-phase symmetrical faults: use of superimposed positive-sequence components.

Excluding the positive-sequence components ($\underline{a}_{F1} = 0$) from the total fault current (4) for all faults, except three-phase balanced faults, is characteristic for the share coefficients from Table II. In case of three-phase balanced faults, only positive-sequence components are contained in the signals. The positive sequence of the total fault current can be calculated as the sum of postfault positive-sequence components from all line terminals. However, it is proposed to calculate it as the following sum of the superimposed (denoted with "Δ") positive-sequence currents from the line ends A, B, and C, respectively:

$$\underline{I}_{F1} = \Delta\underline{I}_{A1} + \Delta\underline{I}_{B1} + \Delta\underline{I}_{C1}. \tag{6}$$

Finally, negative-, zero- and superimposed positive-sequence components of the measured currents are used in the calculation of the total fault current (4). This ensures accurate calculation of the fault current flowing through the fault path resistance. This is so, since the positive-sequence components, for which the shunt capacitance effect is the most distinct, are excluded.

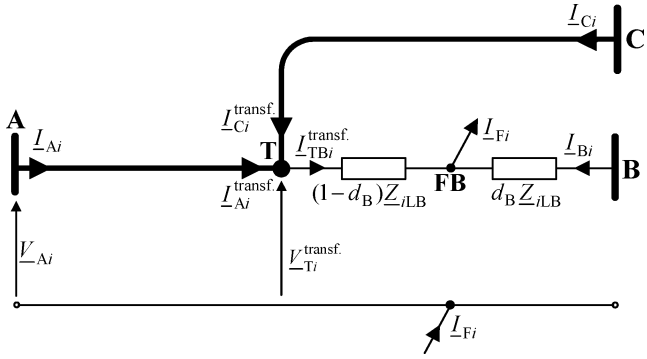

Fig. 3. Circuit diagram of three-terminal line under fault at the section TB, for the ith symmetrical component.

After resolving (1) into the real and imaginary parts, and eliminating the unknown fault resistance (R_{FA}), the sought fault distance (d_A) is determined as

$$d_A = \frac{\text{real}(\underline{V}_{Ap})\text{imag}(\underline{I}_F) - \text{imag}(\underline{V}_{Ap})\text{real}(\underline{I}_F)}{\text{real}(\underline{Z}_{1LA}\underline{I}_{Ap})\text{imag}(\underline{I}_F) - \text{imag}(\underline{Z}_{1LA}\underline{I}_{Ap})\text{real}(\underline{I}_F)}. \tag{7}$$

Having the fault distance calculated (7), the fault resistance R_{FA} can also be determined as, for example, from the real part of (1) as

$$R_{FA} = \frac{\text{real}(\underline{V}_{Ap}) - d_A\text{real}(\underline{Z}_{1LA}\underline{I}_{Ap})}{\text{real}(\underline{I}_F)}. \tag{8}$$

B. Fault-Location Algorithm—Subroutine SUB_B

An analytic transfer of three-phase measurements $\underline{V}_A$, $\underline{I}_A$, and $\underline{I}_C$ to the beginning of the section LB, while strictly taking into account the distributed parameter line model, is performed. The superscript "transf." is used to distinguish the analytically transferred signals from the measured signals. Certainly, such transfer has to be performed separately for each ith type of symmetrical component of three-phase voltage and current. Fig. 3 presents an equivalent circuit diagram of the line for the ith symmetrical component. Again, the subscript "i" is used for denoting the respective $i = 1$ is positive, $i = 2$ is negative, and $i = 0$ the zero sequence components.

Transferring of voltage from the bus A to the tap point T results in

$$\underline{V}_{Ti}^{\text{transf.}} = \cosh(\underline{\gamma}_{i\text{LA}}\ell_{\text{LA}})\cdot\underline{V}_{Ai} - \underline{Z}_{ci\text{LA}}\sinh(\underline{\gamma}_{i\text{LA}}\ell_{\text{LA}})\cdot\underline{I}_{\text{Ai}} \tag{9}$$

where

$\underline{Z}_{ci\text{LA}} = \sqrt{\underline{Z}'_{i\text{LA}}/\underline{Y}'_{i\text{LA}}}$ surge impedance of the line section AT for the ith sequence;

$\underline{\gamma}_{i\text{LA}} = \sqrt{\underline{Z}'_{i\text{LA}}\underline{Y}'_{i\text{LA}}}$ propagation constant of the line section AT for the ith sequence;

$\underline{Z}'_{i\text{LA}}$ impedance of the line section AT for the ith sequence (Ω/km);

$\underline{Y}'_{i\mathrm{LA}}$	admittance of the line section AT for the ith sequence (S/km);
ℓ_{LA}	total length of the section AT (km).

The transfer of the ith symmetrical sequence current from the beginning of the line section LA (bus A) to the end of the section (tap point T) gives

$$\underline{I}_{\mathrm{A}i}^{\mathrm{transf.}} = \frac{-\sinh(\underline{\gamma}_{i\mathrm{LA}}\ell_{\mathrm{LA}})\cdot\underline{V}_{\mathrm{A}i}}{\underline{Z}_{ci\mathrm{LA}}} + \cos(\underline{\gamma}_{i\mathrm{LA}}\ell_{\mathrm{LA}})\cdot\underline{I}_{\mathrm{A}i}. \quad (10)$$

Transfer of the current for the line section TC, performed analogously as in (10), gives $\underline{I}_{\mathrm{C}i}^{\mathrm{transf.}}$ (Fig. 3).

The transferred ith symmetrical sequence current of the faulted line section TB (Fig. 3), flowing from the tap point T toward the fault point FB ($\underline{I}_{\mathrm{TB}i}^{\mathrm{transf.}}$) is calculated as the sum of the currents transferred from the terminals: According to (10)] and from C [analogously as in (10)]

$$\underline{I}_{\mathrm{TB}i}^{\mathrm{transf.}} = \underline{I}_{\mathrm{A}i}^{\mathrm{transf.}} + \underline{I}_{\mathrm{C}i}^{\mathrm{transf.}}. \quad (11)$$

Then, using the determined transferred signals (9), (11), the fault-loop voltage $\underline{V}_{\mathrm{Tp}}$ and current $\underline{I}_{\mathrm{TBp}}$ are composed, analogously as in (2) and (3). In order to determine the distance to fault on the section TB, the following fault-loop model is used:

$$\underline{V}_{\mathrm{Tp}} - (1-d_{\mathrm{B}})\underline{Z}_{1\mathrm{LB}}\underline{I}_{\mathrm{TBp}} - R_{\mathrm{FB}}\underline{I}_{\mathrm{F}} = 0 \quad (12)$$

where

d_{B}	unknown distance to fault on section TB (p.u.) counted from bus B toward fault point FB;
R_{FB}	unknown fault resistance;
$\underline{V}_{\mathrm{Tp}}, \underline{I}_{\mathrm{TBp}}$	fault-loop voltage and current for the subroutine SUB_B;
$\underline{Z}_{1\mathrm{LB}}$	positive-sequence impedance of the section TB;
$\underline{I}_{\mathrm{F}}$	total fault current (formula: (4), (5), Table II).

After resolving (12) into the real and imaginary parts and eliminating the unknown fault resistance (R_{FB}), the sought fault distance (d_{B}) is determined as shown in (13) at the bottom of the page.

Similarly, as in the case of the subroutine SUB_A (8), the fault resistance R_{FA} can be determined as

$$R_{\mathrm{FB}} = \frac{\mathrm{real}(\underline{V}_{\mathrm{Tp}}) - (1-d_{\mathrm{B}})\mathrm{real}(\underline{Z}_{1\mathrm{LB}}\underline{I}_{\mathrm{TBp}})}{\mathrm{real}(\underline{I}_{\mathrm{F}})}. \quad (14)$$

C. Fault-Location Algorithm—Subroutine SUB_C

The subroutine SUB_C, designated for locating faults on the line section TC, is derived analogously to the subroutine SUB_B (Section II-B) and, therefore, is not presented.

D. Improvement of Fault-Location Accuracy

The subroutine SUB_A (presented in Section II-A) is formulated using the lumped model of the line section AT with neglecting shunt capacitances. The subroutine SUB_B (presented in Section II-B) applies the distributed parameter line model only for transferring the signals to the tap point T [(9) and (10)], while the fault-loop model itself (12) is of the lumped character. Analogously, it is for the subroutine SUB_C.

It is important for ensuring high accuracy of fault location that the total fault current in all three subroutines be calculated in such a way that the shunt capacitance effect, which is the most distinct in case of the positive sequence, is minimized.

In view of the aforementioned features of the subroutines, the delivered fault-location algorithm is capable of locating accurate faults if, however, the line sections are not too long.

In case of the length of the line sections above 150 km, similarly as for one-end fault locators [12], a need for improving fault-location accuracy appears.

First, a voltage drop on the faulted segment of the respective line section (Fig. 1: A-FA segment—for subroutine SUB_A; T-FB segment—for subroutine SUB_B; T-FC segment—for subroutine SUB_C) has to be determined by taking into account the distributed parameter line model. This can be accomplished by performing iterative calculations, analogously as in the fault-location algorithm from [12].

Second, further improvement of fault-location accuracy can also be achieved if the total fault current is determined by considering the long line model. For example, considering the flow of currents in the path T-FB-B (Fig. 3), after tedious manipulations on hyperbolic functions, one obtains the following compact formula for the ith symmetrical component of the total fault current:

$$\underline{I}_{\mathrm{F}i} = \frac{-\frac{1}{\underline{Z}_{ci\mathrm{LB}}}\sinh(\underline{\gamma}_{i\mathrm{LB}}\ell_{\mathrm{LB}})\cdot\underline{V}_{\mathrm{T}i} + \cosh(\underline{\gamma}_{i\mathrm{LB}}\ell_{\mathrm{LB}})\cdot\underline{I}_{\mathrm{TB}i} + \underline{I}_{\mathrm{B}i}}{\cosh(\underline{\gamma}_{i\mathrm{LB}}\ell_{\mathrm{LB}}d_{\mathrm{B}})}. \quad (15)$$

Then, this current (15) has to be substituted into (4) and next to the fault-loop model (12). As a result, a nonlinear complex formula is obtained, which can be solved iteratively, using, for example, the Newton–Raphson method.

E. Selection of Valid Subroutine

The presented fault-location algorithm consists of three subroutines and only one of them—the valid subroutine—yields the

$$d_{\mathrm{B}} = \frac{\mathrm{imag}(\underline{V}_{\mathrm{Tp}} - \underline{Z}_{1\mathrm{LB}}\underline{I}_{\mathrm{TBp}})\mathrm{real}(\underline{I}_{\mathrm{F}}) - \mathrm{real}(\underline{V}_{\mathrm{Tp}} - \underline{Z}_{1\mathrm{LB}}\underline{I}_{\mathrm{TBp}})\mathrm{imag}(\underline{I}_{\mathrm{F}})}{\mathrm{real}(\underline{Z}_{1\mathrm{LB}}\underline{I}_{\mathrm{TBp}})\mathrm{imag}(\underline{I}_{\mathrm{F}}) - \mathrm{imag}(\underline{Z}_{1\mathrm{LB}}\underline{I}_{\mathrm{TBp}})\mathrm{real}(\underline{I}_{\mathrm{F}})} \quad (13)$$

results, which correspond to the actual fault. The remaining two subroutines give false results. The multicriteria selection procedure has been developed for selecting the valid subroutine (i.e., for indicating the faulted line section).

In the first step of the selection procedure, the results of the fault distance and resistance calculations are utilized. The subroutine, which yields the distance to fault indicating the considered fault as occurring outside the section range (outside the range: 0 to 1.0 p.u.) and/or the calculated fault resistance of the negative value is surely rejected.

The second step of the selection is used when the first step is not sufficient. In this second step, the remote source impedances (behind the terminals B and C—if it is considered that the fault locator is installed at the station A (Fig. 1), are calculated for different subroutines. For example, in case of considering the subroutine SUB_B (Fig. 3, Section II-B) for locating faults on the line section TB, the source impedance behind the bus B for the positive (negative) sequence is calculated as

$$\underline{Z}_{1\mathrm{SB}}^{\mathrm{SUB\_B}} = \underline{Z}_{2\mathrm{SB}}^{\mathrm{SUB\_B}} = \frac{-\underline{V}_{\mathrm{B2}}^{\mathrm{SUB\_B}}}{\underline{I}_{\mathrm{B2}}} \tag{16}$$

where the estimated voltage at the bus B is equal to

$$\underline{V}_{\mathrm{B2}}^{\mathrm{SUB\_B}} = \underline{V}_{\mathrm{T2}}^{\mathrm{transf.}} - (1-d_{\mathrm{B}})\underline{Z}_{1\mathrm{LB}}\underline{I}_{\mathrm{TB2}}^{\mathrm{transf.}} + d_{\mathrm{B}}\underline{Z}_{1\mathrm{LB}}\underline{I}_{\mathrm{B2}}. \tag{17}$$

In the calculations (16) and (17), the negative-sequence components are used. This can be applied for all faults except three-phase balanced faults, for which the incremental positive-sequence components have to be used.

The source impedance behind the bus C is calculated analogously to (16) and (17). Similarly, the source impedances are calculated according to the subroutine SUB_C.

Having calculated the impedances of the sources behind the remote buses B and C—according to both subroutines (SUB_B, SUB_C), first it is checked in which quadrant of the complex plane they are placed. The actual equivalent source impedance is of the form of R-L branch (i.e., it is considered as being placed in the Ist quadrant of the impedance plane. If the source impedance, calculated according to the considered subroutine, lays outside the Ist quadrant, then this subroutine is false and has to be rejected. Otherwise, if there are still at least two subroutines (out of three) remaining, then the selection has to be continued. The particular subroutine can be rejected also if the calculated value of the remote source differs from the actual impedance. For this purpose, certain knowledge about the actual equivalent sources behind the line terminals has to be possessed.

The presented multicriteria selection procedure will be explained in relation to fault-location results presented further in Section III.

III. ATP–EMTP-Based Evaluation

A. ATP–EMTP Model

An ATP–EMTP software program [14] was applied to evaluate the performance of the developed fault-location algorithm. The modeled 110-kV test network includes the line sections–AT: 100 km, BT: 80 km, TC: 50 km, having the positive- (negative) and zero-sequence impedances

$$\underline{Z}'_{1\mathrm{L}} = (0.0276 + \mathrm{j}0.3151),\ \underline{Z}'_{0\mathrm{L}} = (0.275 + \mathrm{j}1.0265);(\Omega/\mathrm{km}).$$

The equivalent sources $\underline{Z}_{1\mathrm{SA}} = (0.65125 + \mathrm{j}3.693)\Omega$, $\underline{Z}_{0\mathrm{SA}} = (1.159 + \mathrm{j}6.5735)\Omega$, $\underline{Z}_{i\mathrm{SB}} = 2\underline{Z}_{i\mathrm{SA}}$, $\underline{Z}_{i\mathrm{SC}} = 3\underline{Z}_{i\mathrm{SA}}$ were also included.

Existence of the prefault load flow in the modeled network is determined by the assumed phase shift of side B source equal to $-30°$ and side C source $-15°$, with respect to the equivalent source behind bus A (0 °).

TABLE III
Fault-Location Results: a-g Fault on Section at, $R_{\mathrm{FA}} = 10\ \Omega$

$d_{\mathrm{A\_actual}}$ (p.u.)	SUB_A		SUB_B		SUB_C	
	d_{A} (p.u)	R_{FA} (Ω)	d_{B} (p.u.)	R_{FB} (Ω)	d_{C} (p.u.)	R_{FC} (Ω)
0.1	**0.1001**	**9.99**	2.0542	10.22	2.8415	12.17
0.2	**0.2001**	**9.98**	1.8939	10.44	2.6016	13.01
0.3	**0.3001**	**9.96**	1.7428	10.65	2.3631	13.42
0.4	**0.4002**	**9.96**	1.6015	10.81	2.1285	13.47
0.5	**0.5003**	**9.95**	1.4702	10.91	1.9008	13.22
0.6	**0.6005**	**9.96**	1.3499	10.92	1.6833	12.74
0.7	**0.7008**	**9.97**	1.2413	10.82	1.4799	12.10
0.8	**0.8012**	**9.98**	1.1458	10.62	1.2949	11.38
0.9	**0.9018**	**10.00**	1.0649	10.33	1.1333	10.65
For all fault cases the subroutines SUB_B, SUB_C are rejected, while the subroutine SUB_A is selected as the valid one.						

B. Evaluation of the Fault-Location Algorithm

In order to evaluate the derived fault-location algorithm itself, the errorless current and voltage transformers were modeled. Analog antialiasing filters with the cutoff frequency of 350 Hz were included, and 1-kHz sampling frequency was used. Full-cycle Fourier orthogonal filters were applied to determine phasors of the processed signals. The obtained continuous fault-location results were singled by averaging within the postfault interval: from 30 up to 50 ms, after the fault inception.

Different specifications of faults have been considered in the study. However, due to the limited space, only the results for the a–g faults, applied through 10-Ω fault resistance at different locations (0.1 to 0.9 p.u.) on particular line sections (Tables III–VII) are presented here. The performance of the developed fault-location algorithm for the other faults is satisfactory and the fault-location errors are also very low.

For the a-g faults on the line section AT (Table III), only the subroutine SUB_A yields correct results—with the maximal fault location error: 0.0018 p.u. (or: 0.18%), while the other two subroutines are surely rejected as indicating the fault outside their sections range d_{B} and $d_{\mathrm{C}} > 1.0$ p.u.

In case of the a-g faults on the line sections TB (Table IV) and TC (Table V), the subroutine SUB_A yields invalid results ($d_{\mathrm{A}} > 1.0$ p.u.) and, therefore, it is rejected. The other two subroutines (SUB_B, SUB_C) give the fault-location results, which could be accepted $0 < d_{\mathrm{B}}$ and $d_{\mathrm{C}} < 1.0$ p.u., and positive fault resistances R_{FB} and $R_{\mathrm{FC}} > 0\ \Omega$.

In order to judge which subroutine: SUB_B or SUB_C is valid, the selection has to be continued (Table VI and VII). In Table VI, the placement of the calculated impedances of the

TABLE IV
FAULT-LOCATION RESULTS: A-G FAULT ON SECTION TB, $R_{FB} = 10\ \Omega$

d_{B_actual} (p.u.)	SUB_A		SUB_B		SUB_C	
	d_A (p.u.)	R_{FA} (Ω)	d_B (p.u.)	R_{FB} (Ω)	d_C (p.u.)	R_{FC} (Ω)
0.1	2.4997	13.69	**0.0979**	**10.02**	0.6549	6.23
0.2	2.3796	14.12	**0.1982**	**10.01**	0.5878	6.15
0.3	2.2315	14.21	**0.2985**	**10.00**	0.5392	6.28
0.4	2.0690	14.02	**0.3988**	**9.99**	0.5118	6.60
0.5	1.8985	13.59	**0.4991**	**9.98**	0.5087	7.07
0.6	1.7234	13.00	**0.5994**	**9.98**	0.5334	7.64
0.7	1.5457	12.30	**0.6997**	**9.98**	0.5898	8.26
0.8	1.3660	11.53	**0.8000**	**9.97**	0.6827	8.90
0.9	1.1850	10.76	**0.9003**	**9.98**	0.8175	9.49
For all fault cases the subroutine SUB_A is rejected, while the subroutines SUB_B, SUB_C undergo further selection (see Table VI).						

TABLE V
FAULT-LOCATION RESULTS: A-G FAULT ON SECTION TC, $R_{FC} = 10\ \Omega$

d_{C_actual} (p.u.)	SUB_A		SUB_B		SUB_C	
	d_A (p.u.)	R_{FA} (Ω)	d_B (p.u.)	R_{FB} (Ω)	d_C (p.u.)	R_{FC} (Ω)
0.1	1.6406	12.78	0.8723	9.88	**0.0996**	**10.02**
0.2	1.5935	12.88	0.8625	10.05	**0.1999**	**10.01**
0.3	1.5368	12.84	0.8577	10.20	**0.3001**	**10.00**
0.4	1.4731	12.67	0.8583	10.31	**0.4002**	**10.00**
0.5	1.4038	12.39	0.8646	10.37	**0.5004**	**9.99**
0.6	1.3302	12.02	0.8772	10.40	**0.6005**	**9.99**
0.7	1.2528	11.58	0.8964	10.37	**0.7006**	**9.99**
0.8	1.1721	11.09	0.9229	10.29	**0.8007**	**9.98**
0.9	1.0886	10.56	0.9573	10.16	**0.9007**	**9.99**

TABLE VI
SELECTION OF VALID SUBROUTINE: A-G FAULT ON SECTION TB, $R_{FB} = 10\ \Omega$ (FAULT-LOCATION RESULTS IN TABLE IV)

d_{B_actual} (p.u.)	Quadrant of complex plane in which calculated source impedances is placed:				SELECT.
	$\underline{Z}_{1SB}^{SUB\_B}$	$\underline{Z}_{1SC}^{SUB\_B}$	$\underline{Z}_{1SB}^{SUB\_C}$	$\underline{Z}_{1SC}^{SUB\_C}$	
0.1	Ist	Ist	IIIrd	Ist	**SUB_B**
0.2	Ist	Ist	IIIrd	Ist	**SUB_B**
0.3	Ist	Ist	IIIrd	Ist	**SUB_B**
0.4	Ist	Ist	IIIrd	Ist	**SUB_B**
0.5	Ist	Ist	IIIrd	Ist	**SUB_B**
0.6	Ist	Ist	IIIrd	Ist	**SUB_B**
0.7	Ist	Ist	IIIrd	Ist	**SUB_B**
0.8	Ist	Ist	IIIrd	Ist	**SUB_B**
0.9	Ist	Ist	IIIrd	Ist	**SUB_B**

equivalent sources behind buses B and C (denoted at the last position of subscripts), according to the subroutines SUB_B, SUB_C (denoted by superscripts), is shown. For all fault cases, both source impedances are calculated according to the subroutine SUB_B $\underline{Z}_{1SB}^{SUB\_B}$ $\underline{Z}_{1SC}^{SUB\_B}$ lay in the Ist quadrant of the complex plane, while this is not satisfied (IIIrd and Ist quadrant, respectively) for the source impedances $\underline{Z}_{1SB}^{SUB\_C}$, $\underline{Z}_{1SC}^{SUB\_C}$—calculated according to the subroutine SUB_C. As a result, the subroutine SUB_B is selected as the valid, what is consistent with reality (results in Table IV).

Continuing the selection for the faults on the line section LC (fault location results in Table V), the placement of the respective calculated source impedances on the complex plane has been determined. Specification of the complex plane quadrants

TABLE VII
SELECTION OF VALID SUBROUTINE: A-G FAULT ON SECTION TC, $R_{FC} = 10\ \Omega$ (FAULT -LOCATION RESULTS IN TABLE V)

d_{C_actual} (p.u.)	Quadrant of complex plane in which calculated source impedances is placed:				SELECT.
	$\underline{Z}_{1SB}^{SUB\_B}$	$\underline{Z}_{1SC}^{SUB\_B}$	$\underline{Z}_{1SB}^{SUB\_C}$	$\underline{Z}_{1SC}^{SUB\_C}$	
0.1	Ist	IIIrd	Ist	Ist	**SUB_C**
0.2	Ist	IIIrd	Ist	Ist	**SUB_C**
0.3	Ist	IIIrd	Ist	Ist	**SUB_C**
0.4	Ist	IIIrd	Ist	Ist	**SUB_C**
0.5	Ist	IIIrd	Ist	Ist	**SUB_C**
0.6	Ist	IIIrd	Ist	Ist	**SUB_C**
0.7	Ist	IIIrd	Ist	Ist	**SUB_C**
0.8	Ist	IIIrd	Ist	Ist	**SUB_C**
0.9	Ist	Ist	Ist	Ist	**SUB_C**$^{*)}$
$^{*)}$ Selected after applying additional comparison of the calculated source impedances with the actual impedances: $\frac{\lvert \underline{Z}_{1SB}^{SUB\_B} \rvert}{\lvert \underline{Z}_{1SB\_actual} \rvert} = 1.73$; $\frac{\lvert \underline{Z}_{1SC}^{SUB\_B} \rvert}{\lvert \underline{Z}_{1SC\_actual} \rvert} = 0.59$ → SUB_B rejected, $\frac{\lvert \underline{Z}_{1SB}^{SUB\_C} \rvert}{\lvert \underline{Z}_{1SB\_actual} \rvert} = 1.07$; $\frac{\lvert \underline{Z}_{1SC}^{SUB\_C} \rvert}{\lvert \underline{Z}_{1SC\_actual} \rvert} = 1.01$ → SUB_C selected.					

for these impedances is shown in Table VII. Based on this placement, the subroutine SUB_C was selected as the valid for faults occurring on the line section TC at locations $d_{C\_actual} = 0.1$ to 0.8 p.u. For the fault at $d_{C\_actual} = 0.9$ p.u., the subroutine SUB_C was also selected as the valid, just, only after comparing the calculated source impedances with the actual ones (used in modeling). This comparison has shown that the magnitudes of the source impedances calculated according to the subroutine SUB_B are the multipliers: 1.73, 0.59 of magnitudes of the actual impedances. Since these multipliers differ quite distinctly from unity, the subroutine SUB_B was rejected and the subroutine SUB_C remained as the valid. The applied comparison of the calculated source impedances with the actual ones requires knowing the latter. If the utility staff is not able to provide the actual source impedances, then both results still need to be considered to utilize and expedite the line service restoration. For the described fault case (a-g fault on the line section TC at $d_{C\_actual} = 0.9$ p.u.), the following two alternative locations of the fault remain for considering: on the line section TB at $d_B = 0.9573$ p.u. and on the section TC at $d_C = 0.9007$ p.u. Both suppositions indicate the fault as occurring very close to the tap point which is favorable for making the line inspection.

Fault-location results yielded by the subroutines, which were selected as the valid (the results marked in Tables III–V in bold type), are very accurate. The calculated distance to fault (d_A, d_B, d_C) is very close to the actual value of the fault distance $(d_{A\_actual}, d_{B\_actual}, d_{C\_actual})$. The fault-location error does not exceed 0.002 p.u. (0.2%).

C. Comparison of the New Fault-Location Algorithm With the Other Known Algorithm

In order to reveal the superiority of the developed new fault-location algorithm to the others, a quantitative comparison has to be performed. It was taken into account for this comparison that, in principle, the fault-location algorithms belonging to the same category could be taken for comparison. Therefore, the

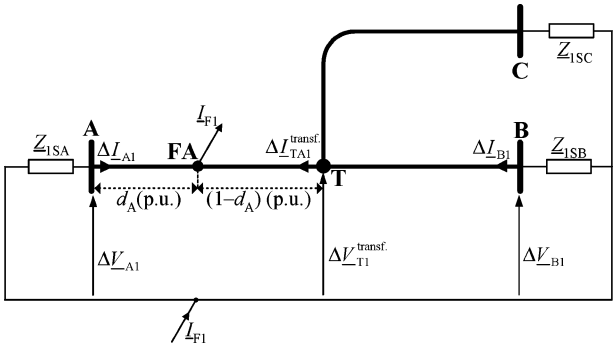

Fig. 4. Illustration for the subroutine SUB_A of the fault-location algorithm from [6].

presented new algorithm was compared to the fault-location algorithm from [6], which also belongs to the category of algorithms utilizing incomplete three-end measurements and using three subroutines and the procedure for selecting the valid subroutine.

Fig. 4 is the illustration for the subroutine SUB_A of the algorithm derived in [6]. The scheme of the network for the superimposed positive sequence (incremental positive sequence), by considering the distributed parameter model of all the line sections is taken into account. From bus A, the superimposed positive-sequence current $(\Delta\underline{I}_{\mathrm{A1}})$ and voltage $(\Delta\underline{V}_{\mathrm{A1}})$ are taken directly as the subroutine SUB_A input signals. Then, the voltage $(\Delta\underline{V}_{\mathrm{T1}}^{\mathrm{transf.}})$ and current $(\Delta\underline{I}_{\mathrm{TA1}}^{\mathrm{transf.}})$ at the tap point T, obtained after the analytic transfer of the measurements acquired at the bus B

$$\Delta\underline{V}_{\mathrm{T1}}^{\mathrm{transf.}} = \cosh(\underline{\gamma}_{\mathrm{1LB}}\ell_{\mathrm{LB}})\Delta\underline{V}_{\mathrm{B1}} - \underline{Z}_{\mathrm{c1LB}}\sinh(\underline{\gamma}_{\mathrm{1LB}}\ell_{\mathrm{LB}})\Delta\underline{I}_{\mathrm{B1}} \quad (18)$$

$$\Delta\underline{I}_{\mathrm{TA1}}^{\mathrm{transf.}} = f(\Delta\underline{I}_{\mathrm{B1}}, \Delta\underline{V}_{\mathrm{B1}}, \underline{\gamma}_{\mathrm{1LB}}, \underline{\gamma}_{\mathrm{1LC}}, \underline{Z}_{\mathrm{c1LB}}, \underline{Z}_{\mathrm{c1LC}}, \ell_{\mathrm{LB}}, \ell_{\mathrm{LC}}, \underline{Z}_{\mathrm{1SC}}). \quad (19)$$

The function (f) determining the current $\Delta\underline{I}_{\mathrm{TA1}}^{\mathrm{transf.}}$ is derived by using a current division theory [6].

Next, using the input signals $\Delta\underline{V}_{\mathrm{A1}}$, $\Delta\underline{I}_{\mathrm{A1}}$, and $\Delta\underline{V}_{\mathrm{T1}}^{\mathrm{transf.}}$ (18), $\Delta\underline{I}_{\mathrm{TA1}}^{\mathrm{transf.}}$ (19), the distance to fault on the section AT is determined according to a simple formula, as in [3].

One can notice that the function (f), determining the current $\Delta\underline{I}_{\mathrm{TA1}}^{\mathrm{transf.}}$ (19), involves the positive-sequence source impedance behind bus C $\underline{Z}_{\mathrm{1SC}}$. The inaccuracy in providing this impedance data (mismatch with respect to the source impedance data) is a source of certain fault-location errors. Table VIII gathers the distance to fault results calculated according to the subroutine SUB_A of the fault-location algorithm from [6] under different mismatch ratios. In case of no mismatch (0% mismatch), the results are very accurate (maximal and average fault-location errors are 0.09% and 0.07%, respectively). However, introducing a certain mismatch with respect to the source impedance $\underline{Z}_{\mathrm{1SC}}$, higher fault location errors appear. For example, for the 50% mismatch (the assumed source impedance is 50% higher than the actual one, with the same phase angle), the maximal and average fault-location errors are: 1.58% and 1.22%, respectively. Even higher fault-location errors appear for the mismatch rate of −50%. If the mismatch rate is within the range (−20%, 20%), then the fault-location errors are kept below 1%, which was also evaluated in [6].

TABLE VIII
COMPARISON OF FAULT-LOCATION ALGORITHMS: a-g FAULT ON SECTION AT, $R_{\mathrm{FA}} = 10\ \Omega$

$d_{\mathrm{A\_actual}}$ (p.u.)	SUB_A: d_{A} (p.u.)					
	FL Algorithm from [6]					New FL Algorithm
	Mismatch Rate:					*)
	0%	50%	20%	-20%	-50%	
0.1	0.1006	0.0912	0.0965	0.1052	0.1135	0.1001
0.2	0.2008	0.1879	0.1952	0.2071	0.2182	0.2001
0.3	0.3009	0.2857	0.2943	0.3083	0.3213	0.3001
0.4	0.4009	0.3844	0.3938	0.4089	0.4228	0.4002
0.5	0.5009	0.4842	0.4937	0.5089	0.5227	0.5003
0.6	0.6008	0.5852	0.5941	0.6083	0.6211	0.6005
0.7	0.7007	0.6872	0.6949	0.7071	0.7180	0.7008
0.8	0.8005	0.7903	0.7962	0.8053	0.8134	0.8012
0.9	0.9003	0.8945	0.8978	0.9029	0.9074	0.9018
$\mathrm{error}_{\mathrm{max}}$	0.09%	1.58%	0.63%	0.89%	2.28%	0.18 %
$\mathrm{error}_{\mathrm{aver}}$	0.07%	1.22%	0.48%	0.69%	1.76%	0.06%
*) There is no mismatch effect						

To distinct the fault-location algorithm from [6], the calculation of the distance to fault according to the presented new fault-location algorithm is not dependent on the source impedances and, thus, there is no mismatch effect. The distance to fault is calculated accurately and the fault-location errors are at the level achieved with the fault location from [6] under precise setting of the source impedance value (0% mismatch).

IV. CONCLUSION

In this work, the new algorithm designed for locating faults on a three-terminal line has been presented. The specific set of the fault-locator input signals has been assumed with the aim of developing the fault-location algorithm for applying current differential relays protecting a three-terminal line. It has been shown that it can be accomplished using phasors of three-phase current from all line terminals—exchanged by the current differential relays, and additionally, the locally measured three-phase voltage phasor.

The developed fault-location algorithm consists of three subroutines, designated for locating faults within the respective line sections, and a multicriteria procedure for selecting the valid subroutine. The subroutines are formulated with the use of generalized fault-loop models. For this purpose, information on the fault type is required. It has been shown that the applied set of the fault-locator input signals allows for accurate determination of the total fault current, flowing through a fault path resistance. Direct summing of currents from all line terminals for particular phases, which is a natural way of determining the total fault current, has not been used in the proposed approach. This is so because since performing direct summing, the positive-sequence currents, for which the shunt capacitances effect is the most distinct, are contained in the summed phase currents. As a result, the accuracy of the total fault current determination deteriorates. Therefore, it has been proposed to determine the total fault current as the weighted sum of particular sequence components, by

applying such a set of the weighted coefficients so that the use of postfault positive-sequence components of currents is avoided.

Three subroutines of the fault-location algorithm have been formulated using the lumped model of the fault loop while neglecting shunt capacitances. The distributed parameter line model was utilized only for the analytical transfer of signals across the healthy line sections toward the tap point. In order to ensure high accuracy of the fault location in case of considerable length of the line sections, the distributed parameter line model has to be fully incorporated to the algorithm. This paper describes how it can be accomplished.

A multicriteria procedure for selecting the valid subroutine has been introduced. First, the subroutine, which yields the distance to fault indicating the considered fault as occurring outside the section range, and/or the calculated fault resistance of a negative value, is rejected. Second, the impedances of the remote sources are calculated according to different subroutines. The placement of a given calculated source impedance outside the Ist quadrant on the impedance plane results in rejecting the considered subroutine. In case this is not sufficient, the comparison of the calculated source impedances with the actual values has to be performed. For this purpose, knowledge with respect to the actual equivalent sources is required. The presented evaluation results show the effectiveness of the proposed selection procedure.

The ATP–EMTP software package was used to demonstrate the performance and advantages of the developed fault-location algorithm. The simulation results show that the accuracy of fault location is very high under various fault types, fault resistances, fault locations, prefault loading conditions, and source impedances. For the presented results for single-phase faults, the achieved accuracy is very high—the fault-location error is less than 0.2% under the assumption of ideal transformation of instrument transformers. Incorporating real models of instrument transformers into the ATP–EMTP model results in certain worsening of fault-location accuracy. However, the delivered fault-location algorithm ensures definitely better accuracy than the one-end approach. This is so since in the presented method, the total fault current is not estimated—for which knowledge of source impedances is required in case of the one-end approach, but is accurately calculated from the measured signals.

REFERENCES

[1] M. S. Sachdev, (coordinator), "Advancements in microprocessor based protection and communication," IEEE Tutorial Publ. No. 97TP120-0, 1997.

[2] *IEEE Guide for Determining Fault Location on AC Transmission and Distribution Lines*, IEEE Std. C37.114, IEEE Power Eng. Soc. Publ., Jun. 8, 2005, pp. 1–42.

[3] R. K. Aggarwal, D. V. Coury, A. T. Johns, and A. Kalam, "A practical approach to accurate fault location on extra high voltage teed feeders," *IEEE Trans. Power Del.*, vol. 8, no. 3, pp. 874–883, Jul. 1993.

[4] A. A. Girgis, D. G. Hart, and W. L. Peterson, "A new fault location technique for two-and three-terminal lines," *IEEE Trans. Power Del.*, vol. 7, no. 1, pp. 98–107, Jan. 1992.

[5] D. A. Tziouvaras, J. Roberts, and G. Benmmouyal, "New multi-ended fault location design for two- or three-terminal lines," in *Proc. 7th Int. Inst. Elect. Eng. Conf. Developments Power Syst. Protection*, April 9–12, 2001, pp. 395–398.

[6] Y. Lin, C. Liu, and C. Yu, "A new fault locator for three-terminal transmission lines using two-terminal synchronized voltage and current phasors," *IEEE Trans. Power Del.*, vol. 7, no. 3, pp. 452–459, Jul. 2002.

[7] J. F. Minambres, I. Zamora, A. J. Mazon, M. A. Zorrozua, and R. Alvarez-Isasi, "A new technique, based on voltages, for fault location on three-terminal transmission lines," *Elect. Power Syst. Res.*, vol. 37, pp. 143–151, 1996.

[8] S. M. Brahma, "Fault location scheme for a multi-terminal transmission line using synchronized voltage measurements," *IEEE Trans. Power Del.*, vol. 20, no. 2, pt. 2, pp. 1325–1331, Apr. 2005.

[9] J. Izykowski, R. Molag, E. Rosolowski, and M. M. Saha, "Fault location in three-terminal line with use of limited measurements," in *Proc. PowerTech (CD)*, St. Petersburg, Russia, Jun. 27–30, 2005.

[10] C. Y. Evrenosoglu and A. Abur, "Travelling wave based fault location for teed circuits," *IEEE Trans. Power Del.*, vol. 20, no. 2, pt. 1, pp. 1115–1121, Apr. 2005.

[11] L. Eriksson, M. M. Saha, and G. D. Rockefeller, "An accurate fault locator with compensation for apparent reactance in the fault resistance resulting from remote-end infeed," *IEEE Trans. Power App. Syst.*, vol. PAS-104, no. 2, pp. 424–436, Feb. 1985.

[12] J. Izykowski, E. Rosolowski, and M. M. Saha, "Locating faults in parallel transmission lines under availability of complete measurements at one end," *Proc. Inst. Elect. Eng., Gen, Transm. Distrib.*, vol. 151, no. 2, pp. 268–273, Mar. 2004.

[13] B. Kasztenny and C. B. Campbell, "Line current differential protective relaying method and relay for in-zone tapped transformers," U.S. Patent, US 6 829 544 B1, Dec. 7, 2004.

[14] H. W. Dommel, *Electro-Magnetic Transients Program*. Portland, OR: BPA, 1986.

Jan Izykowski (M'97–SM'04) was born in Poland in 1949. He received the M.Sc., Ph.D., and D.Sc. degrees from the Faculty of Electrical Engineering of Wroclaw University of Technology (WUT), Wroclaw, Poland, in 1973, 1976, and 2001, respectively.

In 1973, he joined Institute of Electrical Engineering of the WUT. Currently, he is an Associate Professor and Director of WUT. His research interests are in power system transients simulation, power system protection and control, and fault location.

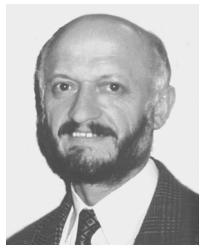

Eugeniusz Rosolowski (M'97–SM'00) was born in Poland in 1947. He received the M.Sc. and D.Sc. degrees in electrical engineering from the Wroclaw University of Technology (WUT), Wroclaw, Poland, in 1972 and 1993, respectively, and the Ph.D. degree from the Kiev Politechnical Institute, Kiev, Ukraine, in 1978.

Currently, he is a Professor in the Institute of Electrical Engineering. His research interests are in power system analysis and microprocessor applications in power systems.

Murari Mohan Saha (M'76–SM'87) was born in Bangladesh in 1947. He received the B.Sc.E.E. and M.Sc.E.E. degrees from Bangladesh University of Engineering and Technology (BUET), Dhaka, India, in 1968 and 1970, respectively, and the M.S.E.E. and Ph.D. degrees from the Technical University of Warsaw, Warsaw, Poland, in 1972 and 1975, respectively.

Currently he is a Senior Research and Development Engineer with ABB Automation Technologies, Västerås, Sweden. His areas of interest are measuring transformers, power system analysis and simulation, and digital protective relays.

Marek Fulczyk (M'04) was born in Poland in 1968. He received the M.Sc. and Ph.D. degrees in electrical engineering from the Wroclaw University of Technology, Wroclaw, Poland, in 1993 and 1997, respectively.

In 1997, he joined ABB as a Research Scientist. Currently, he is a Group Leader of Electrical and Engineering Systems with ABB Corporate Research, Krakow, Poland. His fields of interests include power system protection, power system/voltage stability, real-time collaborative technology, and 3-D modeling and simulations of phenomena in power systems.

Przemyslaw Balcerek was born in Poland in 1976. He received the M.Sc. and Ph.D degrees in electrical engineering from the Wroclaw University of Technology (WUT), Wroclaw, Poland, in 2000 and 2004, respectively.

Currently, he is a Research Scientist with ABB Corporate Research Center, Krakow, Poland. His research interests include fault location, instrument transformers, and ATP–EMTP simulation of power system transients.